In Situ Formation of Frustrated Lewis Pairs in a Zirconium Metal–Organic Cage for Sustainable CO$_2$ Chemical Fixation

Cheng-Xia Chen[1,2], Hassan Rabaâ[1,3], Haiping Wang[1], Pui Ching Lan[1], Yang-Yang Xiong[2], Zhang-Wen Wei[2], Abdullah M. Al-Enizi[4], Ayman Nafady[4] & Shengqian Ma[1*]

[1]*Department of Chemistry, University of North Texas, Denton, Texas 76201,* [2]*MOE Laboratory of Bioinorganic and Synthetic Chemistry, Lehn Institute of Functional Materials, School of Chemistry, Sun Yat-sen University, Guangzhou 510275,* [3]*Department of Chemistry, Ibn Tofail University, ESCTM, 14000 Kenitra,* [4]*Department of Chemistry, College of Science, King Saud University, Riyadh 11451*

Corresponding author: shengqian.ma@unt.edu

Sustainable CO$_2$ fixation represents a facile and promising approach to constructing various value-added chemicals. Herein, we contribute a robust metal–organic cage (MOC), denoted as TCPB-1, comprising a bulky Lewis acid functionalized linker, which can in situ form frustrated Lewis pairs (FLPs) upon the addition of Lewis basic substrates to efficiently drive CO$_2$ transformation. Significantly, the incorporation of Lewis acidic boron sites within TCPB-1 promotes the efficient CO$_2$ conversion to potentially medicinal benzimidazole derivatives via an FLP-mediated pathway, and boosts the stability/durability of the FLP catalyst. In addition, the underlying catalysis mechanism has been established by combined experimental and molecular simulation studies. This work not only advances FLP/MOC as a new type of highly efficient catalyst for CO$_2$ chemical fixation, but also opens a new avenue to design heterogeneous FLP-based catalysts for small molecule activation and beyond.
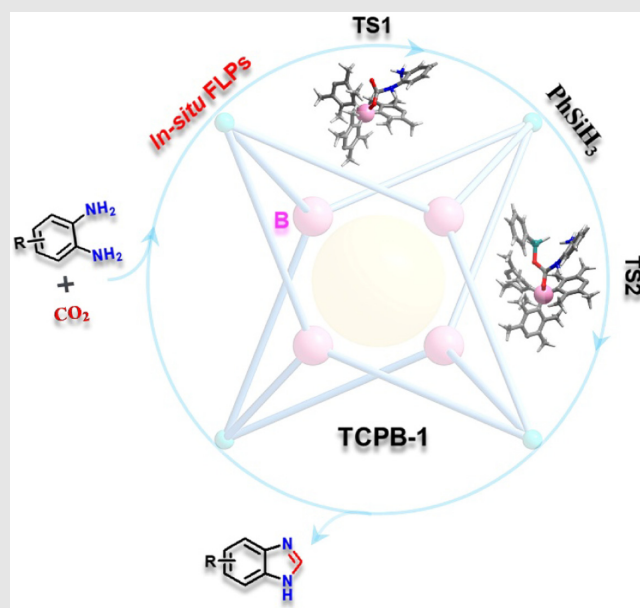
Keywords: metal–organic cage, frustrated Lewis pair, heterogeneous catalysis, CO$_2$ conversion, sustainable chemistry

Introduction

CO_2, as a class of C_1 sources, has been extensively used in synthetic chemistry to gain various valuable chemicals owing to its economical, abundant, as well as nontoxic features.[1-3] Among these, sustainable CO_2 chemical fixation represents a significant research area to tackle global warming concerns.[4-10] Until now, extensive efforts have been devoted to developing functional materials for the production of various chemicals, such as carbonates, methanol (MeOH), amide, etc., by using CO_2 as a C_1 source.[11-22] However, the activation of CO_2 is highly challenging owing to its considerable thermodynamic and kinetic stability, thus impeding the development of the carbon cycle in the pharmaceutical and petroleum industries.

In the past decade, frustrated Lewis pairs (FLPs), comprising a pair of Lewis acid/base in which the steric hindrance of acid or base precludes the formation of the classical donor–acceptor interaction, has drawn tremendous attention owing to their outstanding activation ability for small molecules via metal-free mediated catalysis pathway.[23-36] The unique integration in space endows FLPs with great potential for activating CO_2 molecules arising from its amphiphilic property in which the Lewis acid electrophilically activates oxygen atoms, while the Lewis base bearing nucleophilicity attacks carbon atoms.[34,37-43] The pioneering contribution from the Stephan group described the binding interaction of the FLPs featuring steric phosphines and boranes compounds, with CO_2 yielding zwitterionic products, which opened the avenue for activating CO_2 using FLPs as catalysts.[44] Whereafter, many studies have proved that FLPs can be used as an efficient tool to convert CO_2 to various formyl/acetal/methoxy-borane derivatives, MeOH, methane, etc.[13,23,37-41,43,45-47] Moreover, Sun and colleagues[48] described the $B(C_6F_5)_3$-catalyzed construction of more complicated high-valued benzimidazole derivatives, which involves an FLP-mediated catalysis pathway. These works demonstrate the effectiveness of judicious integration of steric acid/base pairs, presenting enormous potential in catalytic CO_2 chemistry. However, most FLP materials are highly sensitive to moisture, inevitably resulting in dramatic catalyst deactivation. Meanwhile, the homogeneous nature of FLPs not only reduces their catalytic efficiency upon recycling, but also increases the separation complexity of products from the catalytic systems to some extent, thus hindering their broad industrial applicability.

One criterion for designing excellent catalysts is to combine high catalytic activity and outstanding recyclability, which can be achieved through the construction of highly efficient heterogeneous catalysts. However, this remains a challenge for FLPs but is addressable via constructing customized FLP active sites on solid materials.[49-57] Recently, our group described an FLP-functional heterogeneous catalyst through the dynamic installing basic site, 1,4-Diazabicyclo[2.2.2]octane (DABCO), into a metal–organic framework (MOF), followed by introducing the complementary acidic moiety, $B(C_6F_5)_3$, which presented efficient catalytic activity for imine reduction, olefins hydrogenation, and chemoselective hydrogenation of α,β-unsaturated organic compounds, while possessing excellent recyclability.[49,51] Yan and colleagues[55] demonstrated a second-generation CO_2-responsive nano-system by combining the bulky borane- and phosphine-containing building blocks, which can bind CO_2 to form micellar and act as nanocatalysts for highly effective CO_2 conversion. Dyson and co-workers[52] reported a robust MOF constructed from the bulky borane-functional ligand, providing the metal-free and FLP-mediated catalysis pathway for CO_2 conversion. These studies reveal the potential for anchoring FLPs into heterogeneous supports and inspire us to incorporate FLPs into other types of porous materials like metal–organic cages (MOCs), which have been relatively less explored for catalysis.

As a new type of discrete porous material, MOCs, constructed from the coordination of organic linkers and inorganic joints, have been of increasing interest for their recognition, sensing, and separation properties.[58-68] Due to the diversity of organic linkers and inorganic metal nodes, judicious design and coordination engineering can endow MOCs with targeted functional characteristics, such as high stability and effective catalysis activity, thus providing multiple effects on the molecular processes.[68-73] Recently, Zr-MOCs based on strong Zr-O$_{carboxylate}$ bonds have attracted considerable attention owing to their high thermal and chemical stability.[63,67-69,74] Moreover, boron-functional linkers have been extensively used to construct versatile solid catalytic materials,[75-77] arising from the unique electron configuration of boron atoms, $1s^2 2s^2 2p^1$, that is the existence of the vacant 2p orbital, which can serve as a Lewis acid, reacting with a Lewis base to form the FLP for catalysis applications. Along this line, we envision that combining both attributes from Zr-MOCs and boron-functional linkers to design boron-functional Zr-MOCs can not only inherit the advantages of parent species but also impart superior properties that the individual species can hardly realize. Herein, we report a robust MOC, denoted as TCPB-1, constructed from the boron (B)-functional linker, (tris((4-carboxyl)phenyl-duryl)borane, H$_3$L), with bis(cyclopentadienyl)zirconium dichloride, (Cp$_2$ZrCl$_2$, Cp = η^5-C$_5$H$_5$), featuring Lewis acid sites, which can in situ form FLPs upon the addition of basic substrates during the catalysis process. Significantly, TCPB-1 presents efficient catalysis performance for the transformation of *o*-phenylenediamines to high-valued benzimidazole derivatives using CO_2 as the C_1 feedstock. Besides, the catalysis mechanism has been established by combined experimental and molecular simulation studies.
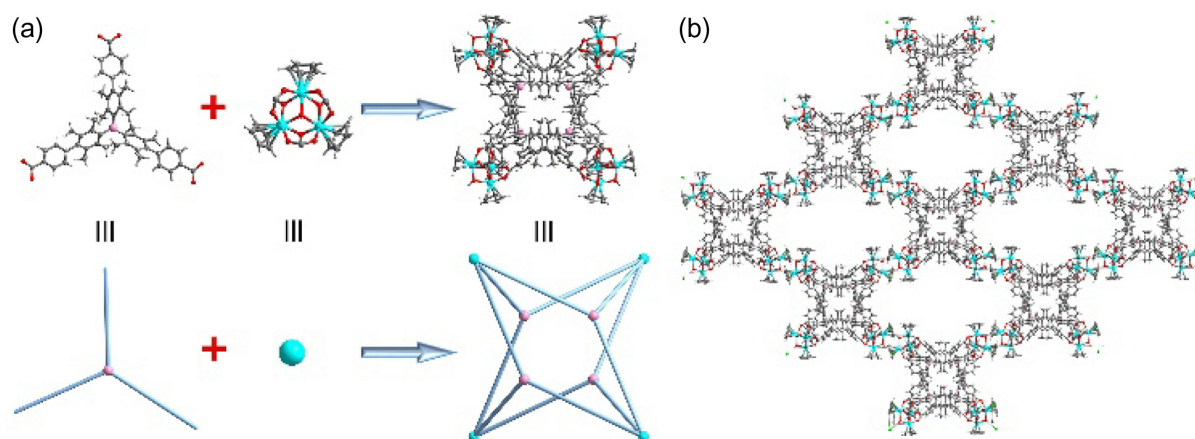
Figure 1 | *The schematic synthetic routine of TCPB-1 and topology analysis. (a) Boron-functional linker, trinuclear $Cp_3Zr_3O(OH)_3$ cluster, the structure of tetrahedral cage. (b) The 3D packing mode of TCPB-1.*

Experimental Methods

Materials and instrumentation

All the reagents and solvents were purchased from commercial sources and directly utilized without further purification. Solid-state infrared (IR) spectra were recorded using a Nicolet/Nexus-670 Fourier transform infrared (FT-IR) spectrometer (Thermo Nicolet Corporation) in the region of 4000–400 cm^{-1} using KBr pellets. Single-crystal X-ray diffraction (SCXRD) data were collected on an Agilent Technologies SuperNova X-RAY diffractometer (Agilent) system equipped with a Cu-sealed tube (λ = 1.54178) at 50 kV and 0.80 mA. Powder X-ray diffraction (PXRD) was carried out with a Rigaku Smart Lab diffractometer (Rigaku; Bragg-Brentano geometry, Cu Kα1 radiation, λ = 1.54056 Å). Thermogravimetric analyses (TGA) were performed on a NETZSCH TG209 system in nitrogen and under 1 atm of pressure at a heating rate of 10 °C min^{-1}. Nuclear magnetic resonance (NMR) data were collected on a 500 MHz NMR spectrometer (Varian). Gas adsorption isotherms for pressures in the range of 0–1.0 bar were obtained by a volumetric method using a Micromeritics ASAP 2020 plus physisorption analyzer (Micromeritics). Gas adsorption measurements were performed using ultra-high purified N_2, and CO_2 gases.

Synthesis of TCPB-1

H_3L (87.5 mg, 0.11 mmol) and zirconocene dichloride (50 mg, 0.17 mmol) were dissolved in *N,N′*-dimethylacetamide (DMAC) (5 mL) and distilled water (750 µL) mixture and then sonicated for 10 min. The mixture was heated at 70 °C for 16 h. After cooling to room temperature, the colorless crystals were harvested and washed with dimethylformamide (DMF) three times. The crystals were immersed in DMF for 24 h during which the solvent

was decanted and freshly replenished every 8 h. Afterwards, the crystals were soaked in acetone for 48 h during which the solvent was decanted and freshly replenished every 8 h. The crystals were collected by filtration and dried at 60 °C for 10 h under a high vacuum.

Computational methods

The reaction mechanism for CO_2 conversion by using TCPB-1 as the catalyst was investigated through density functional theory (DFT) calculations (see details in Supporting Information Figure S13). The X-ray single-crystal crystallographic data were used to perform the parametrizations and simulations.

Results and Discussion

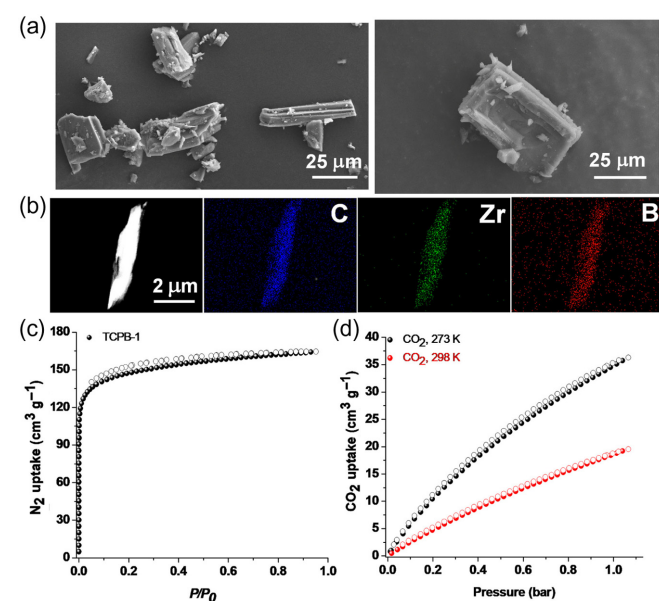### Synthesis and crystal structure description

TCPB-1 was afforded through the solvothermal reaction of H_3L with Cp_2ZrCl_2 in a solvent mixture of DMAC and H_2O at 70 °C for 16 h (Figure 1a). SCXRD analysis revealed that TCPB-1 crystallizes in the orthorhombic system, *Pban* space group, different from the reported ZrT-2.[69] There are one L, one $Cp_3Zr_3O(OH)_3$, and one Cl^- in the asymmetric unit. TCPB-1 is an isolated cationic coordination tetrahedron with a V_4F_4 topology (V = vertex, F = face), in which $Cp_3Zr_3O(OH)_3$ acts as the vertex, whereas the linker L acts as the face (Figure 1a and Supporting Information Figure S1 and Table S1). Due to the introduction of three duryl groups in L, the phenyl rings around the B center twist each other with the dihedral angles of 85.43°, 87.15°, and 88.52°, respectively, thereby resulting in the reduced cage cavity with an aperture of c.a. 5.0 Å (Supporting Information Figure S2). Notably, TCPB-1 is insoluble in common solvents, such as DMF, DMAC, water, tetrahydrofuran (THF), Et_2O, acetonitrile (ACN), and toluene, but has low solubility in

MeOH. In TCPB-1, each isolated tetrahedron cage is connected by four adjacent cages through $H_{OH}\cdots Cl$ (2.06 and 2.17 Å), $H_{cyclopentadiene}\cdots;Cl$ (2.66, 2,79, 2.99, 3.04, 3.14, and 3.62 Å), and $O_{Zr-cluster}\cdots H_{cyclopentadiene}$ (2.71, 2.72, 3.30, and 3.44 Å) hydrogen bonds (Supporting Information Figure S1), thus forming a 3D network with a rhombic channel of approximately 13.6 × 13.6 Å^2 (Figure 1b and Supporting Information Figure S2). After the removal of the solvents in the void, the total accessible volume is estimated to be 63.1% as calculated by PLATON.[78] It is worth noting that the Lewis acidic B center is sterically protected by the bulky duryl groups, which can prevent the strong covalent connection between B and other small donor molecules, like water, as well as preclude the irreversible deactivation of B centers thus bestowing TCPB-1 with the potential to perform FLP-like catalysis.

Phase purity and porosity

The integrity of TCPB-1 was confirmed through electrospray ionization time-of-flight mass spectroscopy (ESI-TOF-MS) studies by solvating the sample in MeOH, which clearly proves the presence of the intact tetrahedron cage in solution (Supporting Information Figure S6). The mass-to-charge ratio value of $[M]^{4+}$ observed at 1303.522 agrees well with the theoretical value based on the chemical composition of TCPB-1. TGA was conducted to assess the thermal stability of TCPB-1, indicating that TCPB-1 is stable up to 400 °C (Supporting Information Figure S4). PXRD patterns were collected to verify the phase purity of the synthesized sample (Supporting

Information Figure S5), as evidenced by the agreement with the calculated PXRD patterns. The scanning electron microscopy (SEM) images show the uniform stick-like morphology of TCPB-1 (Figure 2a). Furthermore, the images of element mapping revealed that C, Zr, and B elements are evenly distributed throughout the whole framework (Figure 2b). To investigate the water stability of TCPB-1, the fresh sample was soaked in water for 48 h. The ESI-TOF-MS analysis confirmed that TCPB-1 retains its framework integrity after treatment with water, indicating its good water stability (Supporting Information Figure S7). N_2 sorption isotherms at 77 K were measured to evaluate the porosity of TCPB-1, which exhibits a type I adsorption behavior with a saturated adsorption amount of 164 cm^3 g^{-1} (Figure 2c and Supporting Information Figure S8). The apparent Brunauer–Emmett–Teller (BET) surface area (S_{BET}) is calculated to be 489 m^2 g^{-1}, corresponding to a total pore volume of 0.25 cm^3 g^{-1} (Supporting Information Table S2). The pore size distribution of TCPB-1 calculated by the DFT is 5.6 and 12.4 Å, agrees well with the pore size observed from the single crystal structure (Supporting Information Figure S11). Besides, the CO_2 sorption isotherms measurements were performed to reveal the good CO_2 adsorption capacity of TCPB-1, which may be beneficial to CO_2 catalytic conversion because of the enrichment effect (Figure 2d). The CO_2 isosteric heat (Q_{st}) for TCPB-1 was calculated to evaluate the host-guest interaction using the Clausius–Clapeyron equation based on the adsorption isotherms at different temperatures with an estimated value of 25.1 kJ mol^{-1} at zero coverage, indicating moderate CO_2-framework interaction (Supporting Information Figures S12 and S13).

Cyclization of benzimidazole derivatives using CO_2 as a C1 source

Given that the cyclization reaction of *o*-phenylenediamine and CO_2 represents one of the most important processes in catalytic CO_2 conversion chemistry, the resulting benzimidazole derivatives are important motifs in natural products and biologically active molecules. We initially assessed the catalytic potential of TCPB-1 by testing the cyclization between commercial *o*-phenylenediamine (**1a**) and CO_2 with hydrosilane as the reductant in a polytetrafluoroethylene (PTFE)-lined autoclave, manifesting that TCPB-1 can drive the cyclization of **1a** to the corresponding benzimidazole (Table 1 and Supporting Information Table S3). The effect of solvents involving aprotic and protonic media was first examined to screen out the most suitable solvent at 120 °C for 24 h. When dichloromethane (DCM), toluene, and tetrahydrofuran (THF) were used as the solvents, the yields of the cyclization were 14%, 21%, and 33%, respectively. When MeOH was used, the yield of benzimidazole (**2a**) increased to 52%. The cyclization proceeded most
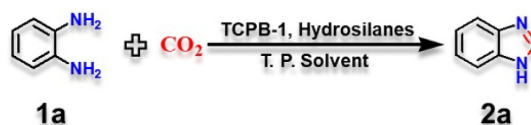

Figure 2 | *(a) The SEM images of TCPB-1. (b) The elemental mappings of C, Zr, and B for TCPB-1. (c) The N_2 adsorption isotherm of TCPB-1. (d) The CO_2 adsorption isotherms at 273 and 298 K.*

Table 1 | *Optimization of the Cyclization Reaction*[a]

Entry	Hydrosilane (equiv)	Solvent	Temp (°C)	TCPB-1 (mol %)	Yield (%)
1	PhSiH$_3$ (4)	DCM	120	5.2	14
2	PhSiH$_3$ (4)	Toluene	120	5.2	21
3	PhSiH$_3$ (4)	THF	120	5.2	33
4	PhSiH$_3$ (4)	MeOH	120	5.2	52
5[b]	Ph$_2$SiH$_2$ (4)	ACN	120	5.2	35
6	PhSiH$_3$ (4)	ACN	120	5.2	92
7[c]	PhSiH$_3$ (4)	ACN	120	5.2	63
8[d]	PhSiH$_3$ (4)	ACN	120	2.0	81
9[e]	PhSiH$_3$ (4)	ACN	80	5.2	65
10[f]	PhSiH$_3$ (1)	ACN	120	5.2	27
11[g]	PhSiH$_3$ (2)	ACN	120	5.2	43
12[h]	PhSiH$_3$ (0)	ACN	120	5.2	—

[a] The reactions were performed in a PTFE-lined autoclave (20 mL) with **1a** (0.2 mmol), hydrosilane (0.8 mmol), and TCPB-1 (5.2 mol %, based on B centers) in solvent (2.0 mL) under CO$_2$ (1.0 MPa) atmosphere.
[b] Reductant-Ph$_2$SiH$_2$.
[c] CO$_2$ pressure-0.5 MPa.
[d] Catalyst loading-0.2%.
[e] Reaction temperature-80 °C.
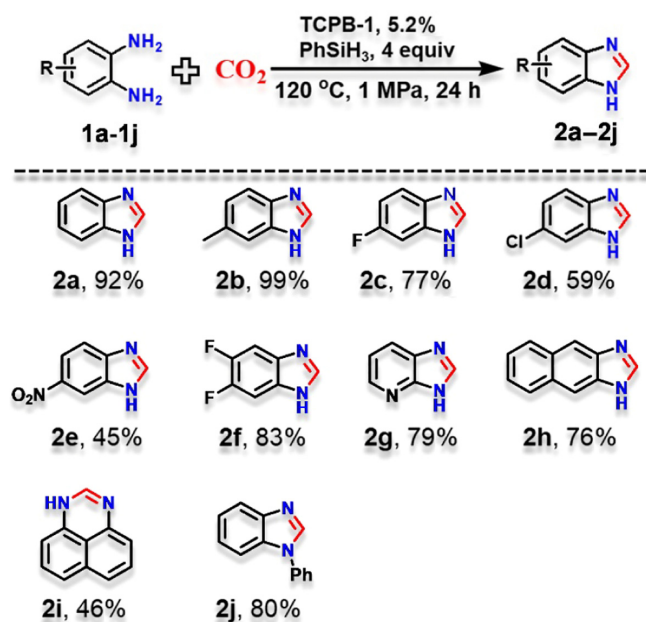[f] PhSiH$_3$-1 equiv.
[g] PhSiH$_3$-2 equiv.
[h] PhSiH$_3$-0 equiv.

efficiently in acetonitrile (ACN), giving a yield of 92%. Afterwards, the optimization of CO$_2$ pressure was carried out in the range of 0.5–1.0 MPa, which revealed that reducing the pressure of CO$_2$ from 1.0 to 0.5 MPa resulted in cyclization yield falling from 92% to 63%. The yield of **2a** slightly decreased from 92% to 81% when reducing the quantity of TCPB-1 from 5.2 to 2.0 mol %. It is worth noting that only marginal cyclization product was observed in the absence of TCPB-1, underscoring the pivotal role of TCPB-1 in promoting the cyclization reaction between *o*-phenylenediamine and CO$_2$. The amount of PhSiH$_3$ serving as the reducing agent also plays an important role in the catalysis process and a steady decrease in conversion from 92% to 27% along with a reduction in the amount of PhSiH$_3$ from 4 to 1 equiv was observed. Notably, the cyclization reaction did not proceed without using PhSiH$_3$, highlighting the important role of hydrosilane as the reducing agent. Further optimization manifested that lowering the reaction temperature or shortening the reaction time resulted in decreased conversion of **1a** into **2a** (Supporting Information Table S3 and Figure S16). Additionally, the substitution of PhSiH$_3$ by Ph$_2$SiH$_2$ as the reducing agent led to drastically decreased conversion.

To assess the general applicability of TCPB-1 as a catalyst in the cyclization reaction, the scope of substrates related to *o*-phenylenediamines was studied under optimized reaction conditions (Table 2). It was found that TCPB-1 was catalytically active toward a variety of *o*-phenylenediamine derivatives bearing electron-donating and -withdrawing groups (Table 2). Notably, the electron effect of substituted groups exerts a significant impact on the reaction efficiency. Specifically, the electron-donating group substituted *o*-phenylenediamine performed smoothly to give the corresponding benzimidazole with a yield of 99%, whereas the electron-withdrawing groups substituted *o*-phenylenediamines furnished the corresponding products with the yield range of 45–77% following the trend of –F > –Cl > –NO$_2$, correlating with the electron-withdrawing effects. The 3,4-difluoride and pyridine functionalized diamines (**1f** and **1g**) can react with CO$_2$ in the presence of TCPB-1 and PhSiH$_3$ to produce the imidazole derivatives **2f** and **2g** with yields of 83% and 79%, respectively. Additionally, the fused naphthalene-based diamine can also be involved in the cyclization reaction, affording 1*H*-naphtho[2,3-*d*] imidazole **2h** with a yield of 76%, while the naphthalene-1,8-diamine performs poorly to the corresponding 1*H*-perimidine with a yield of 46 %. The cyclization of *N*-phenyl-substituted diamine proceeded smoothly to afford the corresponding product **2j** with a yield of 80%. In order to evaluate the durability of

Table 2 | *The Scope of Cyclization of* o-*Phenylenediamine Derivatives with* CO_2 *as a* C_1 *Source*[a]

1a-1j → **2a–2j**

2a, 92%	**2b**, 99%	**2c**, 77%	**2d**, 59%
2e, 45%	**2f**, 83%	**2g**, 79%	**2h**, 76%
2i, 46%	**2j**, 80%		

[a] The reactions were performed in a PTFE-lined autoclave (20 mL) with 1 (0.2 mmol), $PhSiH_3$ (0.8 mmol), and TCPB-1 (5.2 mol %, based on B centers) in ACN (2.0 mL) under CO_2 (1.0 MPa) atmosphere. Isolated yield.

TCPB-1 as a heterogeneous catalyst, recycling experiments were performed under optimized conditions, in which TCPB-1 can be easily separated by filtration followed by washing with methylene chloride and then drying in the air for the next cycle. No significant loss in
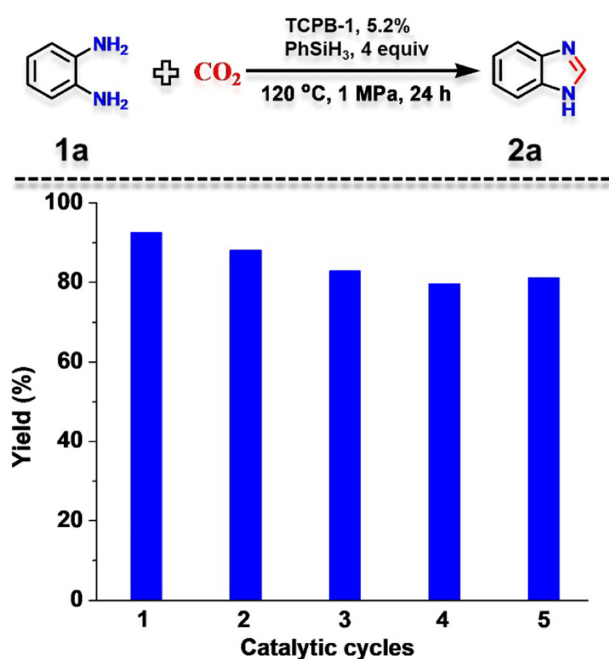

**Figure 3** | *The recycling performance of TCPB-1.*

catalysis activity was observed after five cycles, indicating its excellent reusability/recyclability (Figure 3).

To delineate the reaction mechanism, FT-IR and TGA experiments were performed for TCPB-1 after loading the substrate **1a**, namely **1a**@TCPB-1, revealing no obvious difference between TCPB-1 and **1a**@TCPB-1 (Supporting Information Figures S3 and S4). SCXRD analysis for **1a**@TCPB-1 suggested that no obvious electron cloud was observed near the boron centers. Moreover, the X-ray photoelectron spectroscopy and solid-state ^{11}B CP/MAS NMR analyses were conducted to demonstrate no direct interaction between the boron centers and amino groups, due to the steric hindrance of the duryl groups and the rigidity of TCPB-1 (Supporting Information Figures S14 and S15). To exclude the effect of Zr ions, the BTB-Zr layer constructed from 1,3,5-benzenetrisbenzoate (H_3BTB) and Zr nodes was chosen to implement the cyclization of o-phenylenediamine with CO_2 in the presence of $PhSiH_3$, leading to poor conversion of o-phenylenediamine to benzimidazole.[79,80] It is worth noting that organoboron compounds have been reported to selectively interact with Lewis basic fluoride ions to form [B···F−] pairs, which resulted in the deactivation of boron centers.[52] To evaluate the role of boron centers in the cyclization reaction, the sample of TCPB-1 was soaked in ACN/H_2O solutions containing excess NaF for 2 h, and then filtered and dried in a vacuum oven for 12 h. Subsequently, the cyclization of o-phenylenediamine with CO_2 using the fluoride ion-loaded TCPB-1 under optimized conditions was conducted, showing that the yield of benzimidazole was significantly reduced to 36%, indicative of the vital role of boron centers for the activation of CO_2.

In order to gain further insight into the reaction mechanism, molecular modeling was performed using the DFT[81] through a Gaussian package to manifest an FLP-mediated catalysis reaction pathway (Figure 4). To
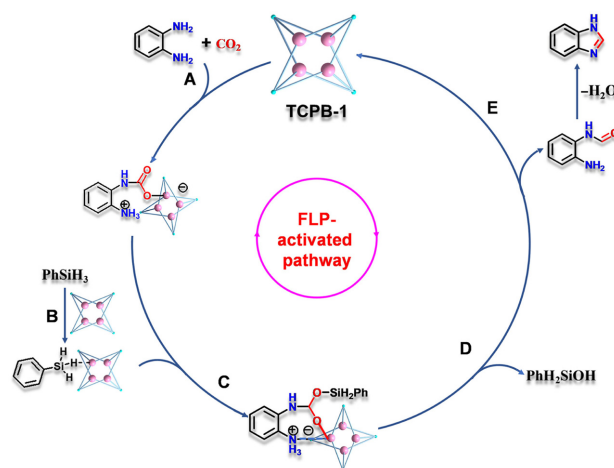
Figure 4 | *Proposed mechanism for the catalytic CO_2 conversion by TCPB-1.*
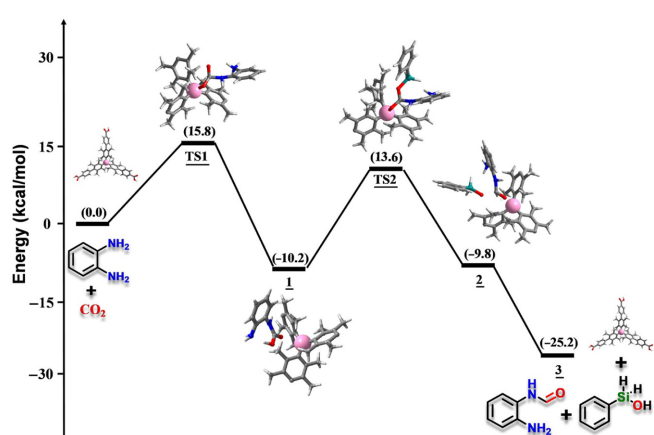
Figure 5 | *Calculated energetic profile at B3LYP/Lanl2dz for the cyclization reaction of* o-*phenylenediamine. Activation energies are given in kcal/mol (between the parenthesis).*

simplify the calculation, the linker stemming from TCPB-1 was used to implement the catalysis. In this study, all molecular structures were fully optimized, under B3LYP/Lanl2dz. Van der Waals interactions were simulated by using the D3(BJ) semi-empirical dispersion correction. Product and reactant geometries were fully optimized using gradient methods. To seek any transition state, quadratic synchronous transit, (QST2 and QST3) with internal reaction coordinate installed as an option in Gaussian 16, was used to ensure that the transition states connect the proposed reactants and products. Calculations were also carried out in the gas phase and solution using ACN as solvent. The Self-Consistent Reaction Field (SCRF) method based on the Solvation Model based on Density (SMD) method has been used. The binding and the Gibbs free energies between the boron functionalized linker and the reactant molecules were calculated at the same level of theory.

As depicted in Figures 4 and 5, DFT calculations were performed on the reaction between boron centers from TCPB-1 and o-phenylenediamine/CO_2 to form N-bound CO_2 adduct **1** (step A). The intermediate product **1** is the result of the combination of proton migration from o-phenylenediamine with the C–O bond activation. Theoretically, this reaction occurs via a transition state, **TS1**, requiring a lower C–O activation estimated to be 15.8 kcal mol^{-1}. The structure of **TS1** showed the different links of H-bonds, i.e., N–H bonds equal to or less than 2.16 Å. The full optimization of **TS1** leads to product **1** with an exothermic reaction profile equal to 10.2 kcal mol^{-1}. Moreover, according to the calculated Mulliken charges of **1**, CO_2 was polarized as [(O=C=O ↔ O=C$^+$–O$^-$)], wherein the Lewis acid electrophilically activates oxygen atoms while the Lewis base bearing nucleophilicity attacks carbon atoms. The second step was the reaction of the reductant $PhSiH_3$ with product **1**, giving rise to the

intermediate product **2**, (steps B and C in Figures 4 and 5). This reaction requires a second transition state, **TS2**, lying with an activation energy of 13.6 kcal mol^{-1} (Figure 5).[81-83] The molecular structure, **TS2**, has a tetrahedral structure with short B–O bonds equaling 1.89 Å and the C–B–C angles were almost equal to 120°, which are imposed by the tetrahedral structure of **TS2** in the cyclization. The reason is the boron configuration, $1s^2 2s^2 2p^1$, involving its lone pair vacant 2p orbital, which can act as a Lewis acid, reacting easily with substrate even at long distances and representing the trait of FLP-mediated catalysis. The intermediate product **2** tends to transform into compound **3** due to the ease of removal for PhH_2SiOH,[21,22] accompanied by a Gibbs free energy release of 35.0 kcal mol^{-1}. Finally, the condensation of compound **3** occurred to afford the desired product, benzimidazole (**2a**), corroborating the experimental data. Notably, the solvation effect also plays a crucial role in the catalysis process, because all energy activation decreased by 5% after the use of ACN solvent. Based on these calculated results, the cyclization seems thermodynamically favored and gives more evidence of the intermolecular reaction between CO_2 and o-phenylenediamine via an FLP-mediated pathway to activate the C–O bonds. Additionally, we assume that the boron site appears to be assisted by the spontaneous formation of the two intermediates (**TS1** and **TS2**). Overall, our results supported the mechanism of the reaction depicted in Figure 4, a plausible mechanism occurs for the formation of benzimidazoles via a FLP pathway from o-phenylenediamine and CO_2 in the presence of TCPB-1. It is ascertained that the solvation also produces a remarkable change in the partial charge distribution at the adsorption centers.

Conclusions

In summary, a robust MOC, TCPB-1, featuring an active boron Lewis acidic center, has been successfully constructed for efficient catalytic conversion of CO_2 to potentially medicinal benzimidazole derivatives through metal-free FLP catalysis pathway, which was established via combined experimental and theoretical calculation studies. This work not only contributes FLP/MOC as a new type of highly efficient catalyst for CO_2 chemical fixation, but also provides a new guideline for the design of heterogeneous FLP-based catalysts for small molecule activation and other challenging chemical transformations.

Supporting Information

Supporting Information is available and includes detailed experimental methods, characterization details, crystallographic data for TCPB-1, catalytic experiments, and theoretical calculations.

Conflict of Interest

There is no conflict of interest to report.

References

1. Banerjee, A.; Dick, G. R.; Yoshino, T.; Kanan, M. W. Carbon Dioxide Utilization via Carbonate-Promoted C-H Carboxylation. *Nature* **2016**, *531*, 215–219.

2. Artz, J.; Mueller, T. E.; Thenert, K.; Kleinekorte, J.; Meys, R.; Sternberg, A.; Bardow, A.; Leitner, W. Sustainable Conversion of Carbon Dioxide: An Integrated Review of Catalysis and Life Cycle Assessment. *Chem. Rev.* **2018**, *118*, 434–504.

3. George, A.; Shen, B.; Craven, M.; Wang, Y.; Kang, D.; Wu, C.; Tu, X. A Review of Non-Thermal Plasma Technology: A Novel Solution for CO_2 Conversion and Utilization. *Renew. Sustain. Energy Rev.* **2021**, *135*, 109702–109782.

4. Abolhasani, M.; Günther, A.; Kumacheva, E. Microfluidic Studies of Carbon Dioxide. *Angew. Chem. Int. Ed.* **2014**, *126*, 8126–8136.

5. Maeda, C.; Miyazaki, Y.; Ema, T. Recent Progress in Catalytic Conversions of Carbon Dioxide. *Catal. Sci. Technol.* **2014**, *4*, 1482–1497.

6. Lang, X. D.; He, L. N. Integration of CO_2 Reduction with Subsequent Carbonylation: Towards Extending Chemical Utilization of CO_2. *ChemSusChem* **2018**, *11*, 2062–2067.

7. Cabrero-Antonino, J. R.; Adam, R.; Beller, M. Catalytic Reductive N-Alkylations Using CO_2 and Carboxylic Acid Derivatives: Recent Progress and Developments. *Angew. Chem. Int. Ed.* **2019**, *58*, 12820–12838.

8. Hong, J.; Li, M.; Zhang, J.; Sun, B.; Mo, F. C-H Bond Carboxylation with Carbon Dioxide. *ChemSusChem* **2019**, *12*, 1–35.

9. Bontemps, S. Boron-Mediated Activation of Carbon Dioxide. *Coord. Chem. Rev.* **2016**, *308*, 117–130.

10. Riduan, S. N.; Zhang, Y. Recent Developments in Carbon Dioxide Utilization Under Mild Conditions. *Dalton Trans.* **2010**, *39*, 3347–3357.

11. Zhou, H.; Zhang, R.; Lu, X.-B. Isolable CO_2 Adducts of Polarized Alkenes: High Thermal Stability and Catalytic Activity for CO_2 Chemical Transformation. *Adv. Synth. Catal.* **2019**, *361*, 326–334.

12. Cui, X.; Shyshkanov, S.; Nguyen, T. N.; Chidambaram, A.; Fei, Z.; Stylianou, K. C.; Dyson, P. J. CO_2 Methanation via Amino Alcohol Relay Molecules Employing a Ruthenium Nanoparticle/Metal Organic Framework Catalyst. *Angew. Chem. Int. Ed.* **2020**, *59*, 16371–16375.

13. Blondiaux, E.; Pouessel, J.; Cantat, T. Carbon Dioxide Reduction to Methylamines Under Metal-Free Conditions. *Angew. Chem. Int. Ed.* **2014**, *53*, 12186–12190.

14. Yu, B.; Zhang, H.; Zhao, Y.; Chen, S.; Xu, J.; Huang, C.; Liu, Z. Cyclization of o-Phenylenediamines by CO_2 in the Presence of H_2 for the Synthesis of Benzimidazoles. *Green Chem.* **2013**, *15*, 95–99.

15. Jacquet, O.; Das Neves Gomes, C.; Ephritikhine, M.; Cantat, T. Complete Catalytic Deoxygenation of CO_2 into Formamidine Derivatives. *ChemCatChem* **2013**, *5*, 117–120.

16. Dobrovetsky, R.; Stephan, D. W. Catalytic Reduction of CO_2 to CO by Using Zinc(II) and in Situ Generated Carbodiphosphoranes. *Angew. Chem. Int. Ed.* **2013**, *52*, 2516–2519.

17. Riduan, S. N.; Zhang, Y.; Ying, J. Y. Conversion of Carbon Dioxide into Methanol with Silanes over N-Heterocyclic Carbene Catalysts. *Angew. Chem. Int. Ed.* **2009**, *48*, 3322–3325.

18. Li, Y.; Fang, X.; Junge, K.; Beller, M. A General Catalytic Methylation of Amines Using Carbon Dioxide. *Angew. Chem. Int. Ed.* **2013**, *52*, 9568–9571.

19. Gao, X.; Yu, B.; Yang, Z.; Zhao, Y.; Zhang, H.; Hao, L.; Han, B.; Liu, Z. Ionic Liquid-Catalyzed C–S Bond Construction Using CO_2 as a C_1 Building Block Under Mild Conditions: A Metal-Free Route to Synthesis of Benzothiazoles. *ACS Catal.* **2015**, *5*, 6648–6652.

20. Bernskoetter, W. H.; Hazari, N. Reversible Hydrogenation of Carbon Dioxide to Formic Acid and Methanol: Lewis Acid Enhancement of Base Metal Catalysts. *Acc. Chem. Res.* **2017**, *50*, 1049–1058.

21. Zhang, X.; Sun, J.; Wei, G.; Liu, Z.; Yang, H.; Wang, K.; Fei, H. In Situ Generation of an *N*-Heterocyclic Carbene Functionalized Metal-Organic Framework by Postsynthetic Ligand Exchange: Efficient and Selective Hydrosilylation of CO_2. *Angew. Chem. Int. Ed.* **2019**, *58*, 2844–2849.

22. Jiang, Y.; Yu, Y.; Zhang, X.; Weinert, M.; Song, X.; Ai, J.; Han, L.; Fei, H. N-Heterocyclic Carbene-Stabilized Ultrasmall Gold Nanoclusters in a Metal-Organic Framework for Photocatalytic CO_2 Reduction. *Angew. Chem. Int. Ed.* **2021**, *60*, 17388–17393.

23. Stephan, D. W. Diverse Uses of the Reaction of Frustrated Lewis Pair (FLP) with Hydrogen. *J. Am. Chem. Soc.* **2021**, *143*, 20002–20014.

24. Paradies, J. Mechanisms in Frustrated Lewis Pair-Catalyzed Reactions. *Eur. J. Org. Chem.* **2019**, *2019*, 283–294.

25. Lam, J.; Szkop, K. M.; Mosaferi, E.; Stephan, D. W. FLP Catalysis: Main Group Hydrogenations of Organic Unsaturated Substrates. *Chem. Soc. Rev.* **2019**, *48*, 3592–3612.

26. Meng, W.; Feng, X.; Du, H. Frustrated Lewis Pairs Catalyzed Asymmetric Metal-Free Hydrogenations and Hydrosilylations. *Acc. Chem. Res.* **2018**, *51*, 191–201.

27. Scott, D. J.; Fuchter, M. J.; Ashley, A. E. Designing Effective 'Frustrated Lewis Pair' Hydrogenation Catalysts. *Chem. Soc. Rev.* **2017**, *46*, 5689–5700.

28. Kehr, G.; Erker, G. Frustrated Lewis Pair Chemistry: Searching for New Reactions. *Chem. Rec.* **2017**, *17*, 803–815.

29. Stephan, D. W. The Broadening Reach of Frustrated Lewis Pair Chemistry. *Science* **2016**, *354*, 1248–1256.

30. Ren, X.; Du, H. Chiral Frustrated Lewis Pairs Catalyzed Highly Enantioselective Hydrosilylations of 1,2-Dicarbonyl Compounds. *J. Am. Chem. Soc.* **2016**, *138*, 810–813.

31. Stephan, D. W.; Erker, G. Frustrated Lewis Pair Chemistry: Development and Perspectives. *Angew. Chem. Int. Ed.* **2015**, *54*, 6400–6441.

32. Stephan, D. W. Frustrated Lewis Pairs: From Concept to Catalysis. *Acc. Chem. Res.* **2015**, *48*, 306–316.

33. Stephan, D. W.; Erker, G. Frustrated Lewis Pair Chemistry of Carbon, Nitrogen and Sulfur Oxides. *Chem. Sci.* **2014**, *5*, 2625–2641.

34. Stephan, D. W.; Erker, G. Frustrated Lewis Pairs: Metal-Free Hydrogen Activation and More. *Angew. Chem. Int. Ed.* **2010**, *49*, 46–76.

35. Chase, P. A.; Welch, G. C.; Jurca, T.; Stephan, D. W. Metal-Free Catalytic Hydrogenation. *Angew. Chem. Int. Ed.* **2007**, *46*, 8050–8053.

36. Chernichenko, K.; Madarasz, A.; Papai, I.; Nieger, M.; Leskela, M.; Repo, T. A Frustrated-Lewis-Pair Approach to Catalytic Reduction of Alkynes to cis-Alkenes. *Nat. Chem.* **2013**, *5*, 718–723.

37. Ashley, A. E.; Thompson, A. L.; O'Hare, D. Non-Metal-Mediated Homogeneous Hydrogenation of CO_2 to CH_3OH. *Angew. Chem. Int. Ed.* **2009**, *48*, 9839–9843.

38. Andreas B.; Warren, E. P.; Parvez, M. Tandem Frustrated Lewis Pair/Tris(pentafluorophenyl)borane-Catalyzed Deoxygenative Hydrosilylation of Carbon Dioxide. *J. Am. Chem. Soc.* **2010**, *132*, 10660–10661.

39. Courtemanche, M. A.; Legare, M. A.; Maron, L.; Fontaine, F. G. Reducing CO_2 to Methanol Using Frustrated Lewis Pairs: On the Mechanism of Phosphine-Borane-Mediated Hydroboration of CO_2. *J. Am. Chem. Soc.* **2014**, *136*, 10708–10717.

40. Wang, T.; Xu, M.; Jupp, A. R.; Qu, Z. W.; Grimme, S.; Stephan, D. W. Selective Catalytic Frustrated Lewis Pair Hydrogenation of CO_2 in the Presence of Silylhalides. *Angew. Chem. Int. Ed.* **2021**, *60*, 25771–25775.

41. Peuser, I.; Neu, R. C.; Zhao, X.; Ulrich, M.; Schirmer, B.; Tannert, J. A.; Kehr, G.; Frohlich, R.; Grimme, S.; Erker, G.; Stephan, D. W. CO_2 and Formate Complexes of Phosphine/Borane Frustrated Lewis Pairs. *Eur. J. Chem.* **2011**, *17*, 9640–9650.

42. Appelt, C.; Westenberg, H.; Bertini, F.; Ehlers, A. W.; Slootweg, J. C.; Lammertsma, K.; Uhl, W. Geminal Phosphorus/Aluminum-Based Frustrated Lewis Pairs: C-H Versus C≡C Activation and CO_2 Fixation. *Angew. Chem. Int. Ed.* **2011**, *50*, 3925–3928.

43. Ménard, G.; Stephan, D. W. Room Temperature Reduction of CO_2 to Methanol by Al-Based Frustrated Lewis Pairs and Ammonia Borane. *J. Am. Chem. Soc.* **2010**, *132*, 1796–1797.

44. Mömming, C. M.; Otten, E.; Kehr, G.; Fröhlich, R.; Grimme, S.; Stephan, D. W.; Erker, G. Reversible, Nicht Metallunterstützte Bindung von Kohlendioxid Durch Frustrierte Lewis-Paare. *Angew. Chem. Int. Ed.* **2009**, *121*, 6770–6773.

45. Sajid, M.; Elmer, L. M.; Rosorius, C.; Daniliuc, C. G.; Grimme, S.; Kehr, G.; Erker, G. Facile Carbon Monoxide Reduction at Intramolecular Frustrated Phosphane/Borane Lewis Pair Templates. *Angew. Chem. Int. Ed.* **2013**, *52*, 2243–2246.

46. Yang, Z.; Yu, B.; Zhang, H.; Zhao, Y.; Ji, G.; Ma, Z.; Gao, X.; Liu, Z. $B(C_6F_5)_3$-Catalyzed Methylation of Amines Using CO_2 as a C_1 Building Block. *Green Chem.* **2015**, *17*, 4189–4193.

47. Chen, J.; Falivene, L.; Caporaso, L.; Cavallo, L.; Chen, E. Y. X. Selective Reduction of CO_2 to CH_4 by Tandem Hydrosilylation with Mixed Al/B Catalysts. *J. Am. Chem. Soc.* **2016**, *138*, 5321–5333.

48. Zhang, Z.; Sun, Q.; Xia, C.; Sun, W. CO_2 as a C_1 Source: $B(C_6F_5)_3$-Catalyzed Cyclization of o-Phenylene-Diamines to Construct Benzimidazoles in the Presence of Hydrosilane. *Org. Lett.* **2016**, *18*, 6316–6319.

49. Niu, Z.; Bhagya Gunatilleke, W. D. C.; Sun, Q.; Lan, P. C.; Perman, J.; Ma, J.-G.; Cheng, Y.; Aguila, B.; Ma, S. Metal-Organic Framework Anchored with a Lewis Pair as a New Paradigm for Catalysis. *Chem* **2018**, *4*, 2587–2599.

50. Yang, J.; Chatelet, B.; Dufaud, V.; Herault, D.; Michaud-Chevallier, S.; Robert, V.; Dutasta, J. P.; Martinez, A. Endohedral Functionalized Cage as a Tool to Create Frustrated Lewis Pairs. *Angew. Chem. Int. Ed.* **2018**, *57*, 14212–14215.

51. Niu, Z.; Zhang, W.; Lan, P. C.; Aguila, B.; Ma, S. Promoting Frustrated Lewis Pairs for Heterogeneous Chemoselective Hydrogenation via the Tailored Pore Environment within Metal-Organic Frameworks. *Angew. Chem. Int. Ed.* **2019**, *58*, 7420–7424.

52. Shyshkanov, S.; Nguyen, T. N.; Ebrahim, F. M.; Stylianou, K. C.; Dyson, P. J. In Situ Formation of Frustrated Lewis Pairs in a Water-Tolerant Metal-Organic Framework for the Transformation of CO_2. *Angew. Chem. Int. Ed.* **2019**, *58*, 5371–5375.

53. Meng, Q.; Huang, Y.; Deng, D.; Yang, Y.; Sha, H.; Zou, X.; Faller, R.; Yuan, Y.; Zhu, G. Porous Aromatic Framework Nanosheets Anchored with Lewis Pairs for Efficient and Recyclable Heterogeneous Catalysis. *Adv. Sci.* **2020**, *7*, 2000067–200075.

54. Deng, Q.; Li, X.; Gao, R.; Wang, J.; Zeng, Z.; Zou, J. J.; Deng, S.; Tsang, S. C. E. Hydrogen-Catalyzed Acid Transformation for the Hydration of Alkenes and Epoxy Alkanes over Co-N Frustrated Lewis Pair Surfaces. *J. Am. Chem. Soc.* **2021**, *143*, 21294–21301.

55. Chen, L.; Liu, R.; Yan, Q. Polymer Meets Frustrated Lewis Pair: Second-Generation CO_2-Responsive Nanosystem for Sustainable CO_2 Conversion. *Angew. Chem. Int. Ed.* **2018**, *57*, 9336–9340.

56. Zhang, Y.; Lan, P. C.; Martin, K.; Ma, S. Porous Frustrated Lewis Pair Catalysts: Advances and Perspective. *Chem Catal.* **2022**, *2*, 439–457.

57. Liu, Q.; Liao, Q.; Hu, J.; Xi, K.; Wu, Y.-T.; Hu, X. Covalent Organic Frameworks Anchored with Frustrated Lewis Pairs for Hydrogenation of Alkynes with H_2. *J. Mater. Chem. A* **2022**, *10*, 7333–7340.

58. Zhang, M. M.; Saha, M. L.; Wang, M.; Zhou, Z. X.; Song, B.; Lu, C. J.; Yan, X. Z.; Li, X. P.; Huang, F. H.; Yin, S. C.; Stang, P. J. Multicomponent Platinum(II) Cages with Tunable Emission and Amino Acid Sensing. *J. Am. Chem. Soc.* **2017**, *139*, 5067–5074.

59. Cai, L. X.; Li, S. C.; Yan, D. N.; Zhou, L. P.; Guo, F.; Sun, Q. F. Water-Soluble Redox-Active Cage Hosting Polyoxometalates for Selective Desulfurization Catalysis. *J. Am. Chem. Soc.* **2018**, *140*, 4869–4876.

60. Fang, Y.; Lian, X.; Huang, Y.; Fu, G.; Xiao, Z.; Wang, Q.; Nan, B.; Pellois, J. P.; Zhou, H. C. Investigating Subcellular Compartment Targeting Effect of Porous Coordination Cages for Enhancing Cancer Nanotherapy. *Small* **2018**, *14*, 1802709–1802719.

61. Fang, Y.; Powell, J. A.; Li, E. R.; Wang, Q.; Perry, Z.; Kirchon, A.; Yang, X. Y.; Xiao, Z. F.; Zhu, C. F.; Zhang, L. L.; Huang, F. H.; Zhou, H. C. Catalytic Reactions Within the Cavity of Coordination Cages. *Chem. Soc. Rev.* **2019**, *48*, 4707–4730.

62. Gao, W. X.; Zhang, H. N.; Jin, G. X. Supramolecular Catalysis Based on Discrete Heterometallic Coordination-Driven Metallacycles and Metallacages. *Coord. Chem. Rev.* **2019**, *386*, 69–84.

63. Lee, H. S.; Jee, S.; Kim, R.; Bui, H.-T.; Kim, B.; Kim, J.-K.; Park, K. S.; Choi, W.; Kim, W.; Choi, K. M. A Highly Active, Robust Photocatalyst Heterogenized in Discrete Cages of Metal–Organic Polyhedra for CO_2 Reduction. *Energy Environ. Sci.* **2020**, *13*, 519–526.

64. Dong, J.; Pan, Y.; Wang, H.; Yang, K.; Liu, L.; Qiao, Z.; Yuan, Y. D.; Peh, S. B.; Zhang, J.; Shi, L.; Liang, H.; Han, Y.; Li, X.; Jiang, J.; Liu, B.; Zhao, D. Self-Assembly of Highly Stable Zirconium(IV) Coordination Cages with Aggregation Induced Emission Molecular Rotors for Live-Cell Imaging. *Angew. Chem. Int. Ed.* **2020**, *59*, 10151–10159.

65. Zhu, Z. K.; Lin, Y. Y.; Yu, H.; Li, X. X.; Zheng, S. T. Inorganic-Organic Hybrid Polyoxoniobates: Polyoxoniobate Metal Complex Cage and Cage Framework. *Angew. Chem. Int. Ed.* **2019**, *58*, 16864–16868.

66. Liu, G.; Di Yuan, Y.; Wang, J.; Cheng, Y.; Peh, S. B.; Wang, Y.; Qian, Y.; Dong, J.; Yuan, D.; Zhao, D. Process-Tracing Study on the Postassembly Modification of Highly Stable Zirconium Metal-Organic Cages. *J. Am. Chem. Soc.* **2018**, *140*, 6231–6234.

67. Jiao, J. J.; Tan, C. X.; Li, Z. J.; Liu, Y.; Han, X.; Cui, Y. Design and Assembly of Chiral Coordination Cages for Asymmetric Sequential Reactions. *J. Am. Chem. Soc.* **2018**, *140*, 2251–2259.

68. Liu, G.; Zeller, M.; Su, K.; Pang, J.; Ju, Z.; Yuan, D.; Hong, M. Controlled Orthogonal Self-Assembly of Heterometal-Decorated Coordination Cages. *Chem. J. Chem.* **2016**, *22*, 17345–17350.

69. Liu, G.; Ju, Z.; Yuan, D.; Hong, M. In Situ Construction of a Coordination Zirconocene Tetrahedron. *Inorg. Chem.* **2013**, *52*, 13815–13817.

70. Zhang, D.; Ronson, T. K.; Zou, Y.-Q.; Nitschke, J. R. Metal–Organic Cages for Molecular Separations. *Nat. Rev. Chem.* **2021**, *5*, 168–182.

71. Hosono, N.; Kitagawa, S. Modular Design of Porous Soft Materials via Self-Organization of Metal–Organic Cages. *Acc. Chem. Res.* **2018**, *51*, 2437–2446.

72. Ahmad, N.; Younus, H. A.; Chughtai, A. H.; Verpoort, F. Metal–Organic Molecular Cages: Applications of Biochemical Implications. *Chem. Soc. Rev.* **2015**, *44*, 9–25.

73. Pan, M.; Wu, K.; Zhang, J. H.; Su, C. Y. Chiral Metal-Organic Cages/Containers (MOCs): From Structural and Stereochemical Design to Applications. *Coord. Chem. Rev.* **2019**, *378*, 333–349.

74. Jiang, Y.; Tan, P.; Qi, S.-C.; Gu, C.; Peng, S.-S.; Wu, F.; Liu, X.-Q.; Sun, L.-B. Breathing Metal–Organic Polyhedra Controlled by Light for Carbon Dioxide Capture and Liberation. *CCS Chem.* **2021**, *3*, 1659–1668.

75. Liu, Y.; Xuan, W.; Zhang, H.; Cui, Y. Chirality- and Threefold-Symmetry-Directed Assembly of Homochiral Octupolar Metal-Organoboron Frameworks. *Inorg. Chem.* **2009**, *48*, 10018–10023.

76. Liu, Y.; Mo, K.; Cui, Y. Porous and Robust Lanthanide Metal-Organoboron Frameworks as Water Tolerant Lewis Acid Catalysts. *Inorg. Chem.* **2013**, *52*, 10286–10291.

77. Xia, Q.; Zhang, J.; Chen, X.; Cheng, C.; Chu, D.; Tang, X.; Li, H.; Cui, Y. Synthesis, Structure and Property of Boron-Based Metal–Organic Materials. *Coord. Chem. Rev.* **2021**, *435*, 213783–213807.

78. Spek, A. L. Single-Crystal Structure Validation with the Program PLATON. *J. Appl. Crystallogr.* **2003**, *36*, 7–13.

79. Wang, Y.; Feng, L.; Pang, J.; Li, J.; Huang, N.; Day, G. S.; Cheng, L.; Drake, H. F.; Wang, Y.; Lollar, C.; Qin, J.; Gu, Z.; Lu, T.; Yuan, S.; Zhou, H.-C. Photosensitizer-Anchored 2D MOF Nanosheets as Highly Stable and Accessible Catalysts Toward Artemisinin Production. *Adv. Sci.* **2019**, *6*, 1802059–1802066.

80. Wang, R.; Wang, Z.; Xu, Y.; Dai, F.; Zhang, L.; Sun, D. Porous Zirconium Metal–Organic Framework Constructed from 2D → 3D Interpenetration Based on a 3,6-Connected kgd Net. *Inorg. Chem.* **2014**, *53*, 7086–7088.

81. Peng, C.; Bernhard Schlegel, H. Combining Synchronous Transit and Quasi-Newton Methods to Find Transition States. *Israel. J. Chem.* **1993**, *33*, 449–454.

82. Rabaâ, H.; Saillard, J. Y.; Hoffmann, R. Hydrogen-Hydrogen and Carbon-Hydrogen Activation Reactions at d0 Metal Centers. *J. Am. Chem. Soc.* **1986**, *108*, 4327–4333.

83. Cundari, T. R.; Pierpont, A. W.; Rabaâ, H. Carbon–Hydrogen Versus Carbon–Heteroatom Activation by a High-Valent Zirconium-Imido Complex. *Int. J. Quant. Chem.* **2006**, *106*, 1611–1619.